Available online at www.sciencedirect.com
ScienceDirect
Trans. Nonferrous Met. Soc. China 35(2025) 377−391
Transactions of Nonferrous Metals Society of China
www.tnmsc.cn

First-principles study of physical properties of $L1_2$-Al_3X structural phases for heat-resistant aluminum conductors

Yao-jie KONG[1], Hong-ying LI[1,2,3], Hui-jin TAO[1], Wen-jian LIU[1]

1. School of Materials Science and Engineering, Central South University, Changsha 410083, China;
2. State Key Laboratory on Lightweight High-strength Structural Material, Central South University, Changsha 410083, China;
3. Key Laboratory of Nonferrous Metal Materials Science and Engineering, Ministry of Education, Central South University, Changsha 410083, China

Received 4 July 2023; accepted 29 February 2024

Abstract: The mechanical, thermodynamic properties and electrical conductivities of $L1_2$-Al_3X (X=Zr, Sc, Er, Yb, Hf) structural phases in aluminum conductors were investigated through a first-principles study. The results demonstrate that all structural phases have good alloy-forming ability and structural stability, where Al_3Zr is the most superior. Al_3Zr, Al_3Hf and Al_3Sc have enhanced shear and deformation resistance in comparison to other phases. Within the temperature range of 200−600 K, Al_3Er and Al_3Yb possess the greatest thermodynamic stability, followed by Al_3Hf, Al_3Zr and Al_3Sc. Al_3Er and Al_3Yb have higher thermodynamic stability than Al_3Hf, Al_3Zr and Al_3Sc. All structural phases exhibit substantial metallic properties, indicating their good electrical conductivity. The electrical conductivities of Al_3Hf and Al_3Zr are higher than those of Al_3Er, Al_3Yb and Al_3Sc. The covalent bond properties in Al_3Sc, Al_3Er and Al_3Yb enhance the hardness, brittleness and thermodynamic stability of the structural phase. The thermodynamic stability of Al_3Sc is significantly reduced by ionic bonds.

Key words: aluminum conductor; $L1_2$-Al_3X structural phase; first-principles; mechanical properties; thermodynamic properties; electrical conductivity; valence bonds

1 Introduction

Aluminum (Al) conductors are considered crucial materials for the construction of high-capacity, long-range and low-loss transmission lines owing to their exceptional electrical conductivities and specific strength. Nevertheless, there is a conflict between conductivity and strength, heat resistance, hence imposing significant constraints on the continued advancement of conductors in the realm of transmission [1,2]. The pursuit of developing Al alloys with enhanced strength, conductivity and heat resistance has emerged as a significant need in China's efforts to construct a secure and efficient energy infrastructure [3]. The uniform dispersion of high-hardness Al_3X phases throughout the alloy can be achieved by incorporating micro-alloying materials into Al and subjecting it to the suitable heat treatment. The degree of misfit between the Al_3X phases and the matrix is minimal. Specifically, the Al_3X phases exhibiting an $L1_2$ crystal structure have the ability to establish a cohesive interface with the matrix. This interface aims to reduce surface energy while simultaneously maximizing the strengthening effect. It is an ideal dispersion-strengthening phase for heat-resistant Al conductors [4,5].

Corresponding author: Hong-ying LI, E-mail: lhying@csu.edu.cn
DOI: https://doi.org/10.1016/S1003-6326(24)66686-0

Several studies have incorporated micro-alloying elements, including Zr [6], Er [7], Sc [8], Hf [9,10] and Yb [11] into Al alloys. The stable existence of the $L1_2$-Al_3X (X = Zr, Er, Sc, Hf, Yb) structural phases in the alloys has been discovered. This not only serves to assure the conductivities of the alloys, but also enhances their strength and heat resistance. Furthermore, it has been shown that the physical properties (mechanical properties, thermodynamic properties and electrical conductivities) of different $L1_2$-Al_3X phases exhibit variations. Additionally, their respective impacts on enhancing the qualities of Al alloys are not uniform [12,13]. The physical properties of structural phases are not easily characterized by experiments [14]. The utilization of density functional theory in the first-principles calculation allows for a comprehensive understanding of electronic interactions and valence bonds among atoms in various structural phases. Consequently, this approach enables precise predictions of the physical properties associated with these phases. PAN et al [15] conducted a first-principles analysis to determine the mechanical and thermodynamic properties of $L1_2$-Al_3X (Er, Yb) phases. Their findings provide evidence that these phases exhibit notable strength even under elevated temperature conditions. LAN et al [16] analyzed the mechanical and thermodynamic properties of $L1_2$-Al_3X (Zr, Sc, Er, Hf, Yb) phases. Their findings reveal that $L1_2$-Al_3X (Er, Yb) exhibits advantageous qualities in terms of enhancing the heat resistance of the alloy. FAN et al [17] conducted high-throughput calculations to determine the electrical conductivities of Al and $L1_2$-Al_3X (Sc, Er, Yb) phases. The results show that the conductivities of the structural phases are in the order of Al_3Sc > Al_3Yb > Al_3Er. Additionally, the conductivity of Al exhibits a modest increase as the temperature rises. CUI et al [18] employed first-principles calculations to ascertain the conductivity of Al, and their findings reveal a consistent decline in conductivity as temperature increased. However, the majority of existing research on the conductor's $L1_2$-Al_3Zr structure is devoted to comparing mechanical and thermodynamic properties, with no definitive research on the electrical conductivity. At the same time, there is a lack of comprehensive research on the mechanical properties, thermodynamic properties and electrical conductivities of structural phases. In this work, the mechanical and thermodynamic properties of $L1_2$-structural phases (Al_3Zr, Al_3Er, Al_3Sc, Al_3Hf and Al_3Yb) were calculated theoretically in the temperature range where phase stability exists [5,19]. The electrical conductivities of structural phases were characterized using electronic structures, and the distinctions in properties among these phases were examined based on the essence of chemical bonds. This analysis offers theoretical backing for the subsequent development of Al conductors with superior conductivity, strength and heat resistance.

2 Computational method and model

2.1 Computational method

The properties were calculated by the utilization of the first-principles plane-wave pseudo-potential Vienna Ab-initio Simulation Package (VASP) [20]. The projector augmented wave (PAW) method was used to describe the ion-electron interactions [21]. The treatment of the exchange-correlation functional involved the utilization of the generalized gradient approximation (GGA) proposed by Perdew-Burke-Ernzerhof (PBE) [22].

Unless otherwise specified, all phases were fully relaxed with respect to volume as well as all cell–internal atomic coordinates. The convergence of results with respect to the energy cutoff, k points and energy broadening sigma was carefully considered. The energy cutoff and smearing width were chosen to be 450 eV and 0.2 eV, respectively. The Monkhorst−Pack method was used to mesh k points, with a density of which was less than 0.03 [23]. A convergence criterion of less than 1 meV/atom was employed to determine the relative energy difference. The self-consistent convergence criterion for electron iterations was set at the value of 10^{-5} eV/atom, and the electron occupation was described using the first-order Methfessel−Paxton scheme. The atomic geometries in their ground state were optimized by the process of minimizing the Hellmann−Feynman force. This optimization was continued until the total force acting on each ion reached a converged value of 0.01 eV/Å. The Birch−Mürnaghan equation of state (EOS) was utilized to elucidate the correlation between energy and volume. In general, the strong correlation of f electrons has a substantial influence on the calculation of oxide, nitride and insulator systems. Conversely, the extent of electron

localization in metal systems is small, so the impact of *f* electrons in rare earths on the calculation of metal compounds is not considered [16]. The valence configurations of the elements were as follows: Al-$3s^2 3p^1$, Zr-$4s^2 4p^6 4d^2 5s^2$, Er-$5s^2 5p^6 6s^2$, Sc-$3s^2 3p^6 3d^1 4s^2$, Hf-$5p^6 5d^2 6s^2$, and Yb-$4d^1 5p^6 6s^2$ [24].

Combining the crystal structure phonon calculation software module, Phonopy, allowed for the computation of the thermodynamic parameters of the structural phase [25]. The calculation method is based on density functional perturbation theory (DFPT) [26]. Considering the anharmonic effect in the process of lattice vibration, the change of potential field caused by the movement of atoms was obtained. Based on this, the kinetic matrix was constructed and the corresponding thermodynamic properties were finally obtained. These properties include the phonon density of states, free energy, enthalpy and entropy, among others. The quasi-harmonic approximations (QHA) method was employed to obtain the specific heat at constant pressure [27].

2.2 Computational model

The $L1_2$-Al_3X exhibits a Cu_3Au crystal structure, which belongs to the space group of $Pm\bar{3}m$. This structure contains four atoms (Fig. 1). The primitive cell approach was used for structural relaxation analysis, while the supercell approach was used for phonon spectrum (3×3×2) and charge density (2×2×1) analysis.

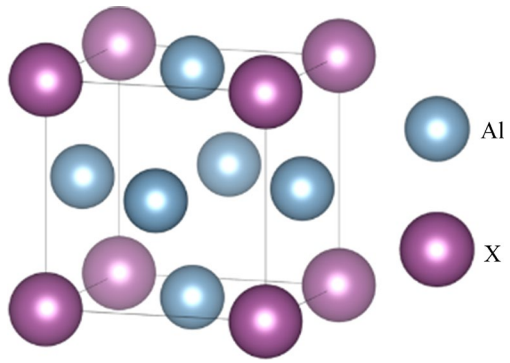

Fig. 1 Crystal structure of $L1_2$-Al_3X structural phases (X=Zr, Sc, Er, Yb, Hf)

3 Results and discussion

3.1 Lattice parameter

The ground state parameters for pure metals, Al, Zr, Er, Sc, Hf, Yb, and the $L1_2$-Al_3X structural phases, were calculated. The lattice parameters obtained by calculations for the $L1_2$-Al_3X phases are compared with the values reported in the literature, as presented in Table 1. The derived relevant parameters exhibit a high level of concordance with the computed and experimental findings reported in existing scholarly literature. The discrepancy in the experimental data is below 1%. Hence, the present calculation parameters enable precise prediction of the mechanical properties, thermodynamic properties and electronic structure of $L1_2$-Al_3X phases.

Table 1 Lattice parameters comparison of $L1_2$-Al_3X structural phases with literature

Phase	Lattice parameter/Å		
	Present	Calculation	Experiment
Al_3Zr	4.105	4.097 [28], 4.12 [29], 4.107 [30]	4.09 [31], 4.117 [32]
Al_3Er	4.231	4.232 [33], 4.23 [34], 4.215 [35]	4.22 [5], 4.215 [36], 4.214 [37]
Al_3Sc	4.106	4.038 [38], 4.106 [33], 4.103 [39]	4.106 [40], 4.110 [14]
Al_3Hf	4.089	4.0807 [14], 4.091 [41]	4.048 [5], 4.08 [41]
Al_3Yb	4.212	4.1906 [14], 4139 [42], 4.295 [5]	4.200 [14], 4.219 [42]

3.2 Formation enthalpy and binding energy

The formation enthalpy serves as a crucial parameter in assessing the alloy-forming ability of $L1_2$-Al_3X structural phases. It is used to characterize the energy released (or absorbed) by atoms during the formation of compounds from elementary substances, as shown in Eq. (1) [43]:

$$\Delta H(Al_3X) = E(Al_3X) - \left[\frac{3}{4}E(Al) + \frac{1}{4}E(X)\right] \quad (1)$$

where $E(Al_3X)$, $E(Al)$ and $E(X)$ represent the energy of a single atom in $L1_2$-Al_3X structural phases, Al and X elements after full relaxation, respectively. The unit is eV/atom.

The binding energy is defined as the energy required to decompose the compound into a single atom. It is used to reflect the strength of atomic

binding in $L1_2$-Al_3X structural phases, as shown in Eq. (2) [44]:

$$E_{\mathrm{coh}}(\mathrm{Al_3X}) = E(\mathrm{Al_3X}) - \left[\frac{3}{4}E(\mathrm{Al})_{\mathrm{atom}} + \frac{1}{4}E(\mathrm{X})_{\mathrm{atom}}\right] \quad (2)$$

where E(Al) atom and E(X) atom represent the energy of isolated Al and X atoms after full relaxation, respectively. The unit is eV/atom.

Table 2 displays the formation enthalpy and binding energy of several structural phases, exhibiting a strong agreement with the calculated and experimental findings documented in the existing literature. As the formation enthalpy becomes more negative, the bonding energy and the alloy-forming ability of the structure become stronger. The order of the negative formation enthalpy of the structural phases from large to small is Al_3Zr, Al_3Sc, Al_3Er, Al_3Yb and Al_3Hf (<0), which suggests a favorable alloy-forming capability for these phases. Al_3Zr is the most superior performance among them. The negative value of binding energy indicates that structural phases can exist stably. The more stable the crystal structure, the larger the negative value of binding energy [53]. The order of the negative binding energies of the structural phases from large to small is Al_3Zr, Al_3Hf, Al_3Er, Al_3Sc, and Al_3Yb (<0). This order highlights the remarkable structural stability of these phases, with Al_3Zr displaying the highest performance among them.

Table 2 Enthalpy of formation (ΔH) and binding energy (E_{coh}) of $L1_2$-Al_3X structural phases

Phase	ΔH/(eV·atom^{-1})		E_{coh}/(eV·atom^{-1})	
	Present	Calculation	Present	Calculation
Al_3Zr	−0.4618	−0.4811 [28], −0.4622 [41]	−4.672	−4.857 [45], −5.37 [46]
Al_3Er	−0.4154	−0.4146 [47], −0.4239 [48]	−4.148	−4.45 [49], −4.930 [42]
Al_3Sc	−0.4543	−0.4643 [50], −0.4509 [40]	−4.118	−4.19 [45], −4.67 [46]
Al_3Hf	−0.3656	−0.378 [51], −0.382 [14]	−4.632	−4.962 [51]
Al_3Yb	−0.4097	−0.373 [42], −0.3368 [52]	−4.100	−4.445 [42]

3.3 Elastic properties

The independent elastic constants can indicate the crystal's capability to withstand elastic deformation and external stress. According to the Hooke's law, the relationship between stress and strain is linear under small distortion. The stress component can be described as a linear function of the strain component, and the matrix is expressed as

$$\sigma_i = C_{ij} \cdot e_j \quad (3)$$

where σ_i is the stress tensor element, e_j is the strain tensor element, and C_{ij} is the elastic modulus tensor element. The $L1_2$ structure phase belongs to the cubic crystal system and has high symmetry, its elastic modulus matrix is [54]

$$\begin{bmatrix} C_{11} & C_{12} & C_{12} & 0 & 0 & 0 \\ C_{12} & C_{11} & C_{12} & 0 & 0 & 0 \\ C_{12} & C_{12} & C_{11} & 0 & 0 & 0 \\ 0 & 0 & 0 & C_{44} & 0 & 0 \\ 0 & 0 & 0 & 0 & C_{44} & 0 \\ 0 & 0 & 0 & 0 & 0 & C_{44} \end{bmatrix} \quad (4)$$

There are three non-zero elastic constants C_{11}, C_{12} and C_{44} [55]. The results are listed in Table 3.

The characterization of a material's ability to endure deformation under uniaxial strain can be achieved using C_{11}. The shear resistance of materials along the (00l) (l is the crystal plane index)

Table 3 Independent elastic constants of $L1_2$-Al_3X structural phases

Phase	C_{11}/GPa		C_{12}/GPa		C_{44}/GPa	
	Present	Calculation	Present	Calculation	Present	Calculation
Al_3Zr	181.29	182.2 [56], 179.3 [29]	64.92	67.9 [56], 64.0 [29]	71.35	72.5 [56], 72.8 [29]
Al_3Er	159.10	159.59 [15], 160.05 [50]	37.60	36.33 [15], 36.52 [50]	61.30	62.64 [15], 60.95 [50]
Al_3Sc	180.17	181.6 [57], 191 [38], 183.0* [38]	36.68	41.6 [57], 43 [38], 46.0* [38]	71.50	69.3 [57], 82 [38], 68.0* [38]
Al_3Hf	180.87	176.88 [56], 176.6 [51]	65.02	68.23 [56], 69.2 [51]	70.62	68.6 [56], 68.5 [51]
Al_3Yb	162.19	158.27 [15], 135.47 [42]	37.87	38.01 [15], 45.59 [42]	62.48	61.76 [15], 80.19 [42]

*Experimental data

and the ⟨111⟩ four-degree axis can be characterized by C_{12} and C_{44}, respectively. The standard conditions for mechanical stability are expressed as follows [58]: $C_{11} > 0$, $C_{12} > 0$, $C_{11} - C_{12} > 0$, $C_{11} + 2C_{12} > 0$. The results show that the structural phases satisfy the requirements for mechanical stability. Further analysis of the elastic constants reveals that Al_3Zr, Al_3Hf and Al_3Sc have superior resistance to deformation and shear in comparison to Al_3Yb and Al_3Er.

In practical applications, the elasticity capacity of materials is commonly characterized by the elastic moduli, including the bulk modulus (B) and shear modulus (G). The elastic moduli can be determined by utilizing the elastic constants derived through the VRH approximation (Voigt−Reuss−Hill approximate model) [59], as shown in Eqs. (5)−(8):

$$B=B_V=B_R=\frac{C_{11}+2C_{12}}{3} \tag{5}$$

$$G_V=\frac{C_{11}-C_{12}+C_{44}}{5} \tag{6}$$

$$G_R=\frac{5c_{44}(C_{11}-C_{12})}{4C_{44}+3(C_{11}-C_{12})} \tag{7}$$

$$G=\frac{G_V+G_R}{2} \tag{8}$$

where B, B_V, B_R, G, G_V and G_R represent the bulk modulus and shear modulus obtained by Hill, Voigt, Reuss methods, respectively.

Young modulus (E) and Poisson ratio (v) can be determined using Eqs. (9) and (10):

$$E=\frac{9BG}{3B+G} \tag{9}$$

$$v=\frac{E}{2G}-1 \tag{10}$$

Table 4 displays the computed elastic parameters of $L1_2$-Al_3X structural phases. The results exhibit a close agreement with the findings published in the literature. The analyses of bulk modulus, shear modulus and Young modulus further demonstrate that Al_3Zr, Al_3Hf and Al_3Sc have superior elastic capacity compared to Al_3Yb and Al_3Er. The transition from ductile-to-brittle structural phases in a cubic crystal can be quantified using the Cauchy pressure ($C_{12}-C_{44}$) [64], the Pugh value (B/G) [65] and v. When $C_{12}-C_{44} < 0$, $B/G < 1.75$ and $v < 0.26$, these conditions suggest that the material exhibits brittle behavior. On the contrary, the material will exhibit ductility. Based on the comparison presented in Fig. 2, it can be observed that all the $L1_2$-Al_3X structural phases exhibit brittleness. The ranking of brittleness, in descending order, is as follows: Al_3Sc, Al_3Er, Al_3Yb, Al_3Zr and Al_3Hf. The brittleness propensity of Al_3Er and Al_3Sc exhibits similarity.

3.4 Hardness

The measurement of hardness serves as a significant mechanical characteristic in the assessment of a material's ability to resist wear. It is often used to indirectly evaluate the strength of aluminum alloys. The estimation of the hardness of $L1_2$-Al_3X structural phases can be derived using the obtained elastic moduli from Eq. (11) [58].

Table 4 Elastic modulus of $L1_2$-Al_3X structural phases

Phase	B/GPa		G/GPa		E/GPa		v	
	Present	Calculation	Present	Calculation	Present	Calculation	Present	Calculation
Al_3Zr	103.71	102.6 [60], 103.5 [61]	65.76	66.7 [60], 69.7 [61]	162.85	164.5 [60], 170.7 [61]	0.238	0.233 [60], 0.225 [61]
Al_3Er	78.10	77.7 [62], 77.42 [32]	61.10	61.28 [62], 62.24 [15]	145.40	145.56 [62], 147.25 [15]	0.171	0.188 [50]
Al_3Sc	84.51	88.24 [50], 91.7* [38]	71.60	69.62 [50], 68.2* [38]	167.50	166 [63], 165.4 [50]	0.170	0.2 [63], 0.188 [50]
Al_3Hf	103.64	104.5 [56], 105 [51]	65.24	62.7 [56], 62.2 [51]	161.76	155.8 [51]	0.240	0.249 [56], 0.25 [51]
Al_3Yb	79.31	78.1 [15], 75.55 [42]	62.35	61.11 [15], 63.56 [42]	148.21	145.4 [15], 112.5 [42]	0.189	0.243 [42], 0.138 [49]

*Experimental data

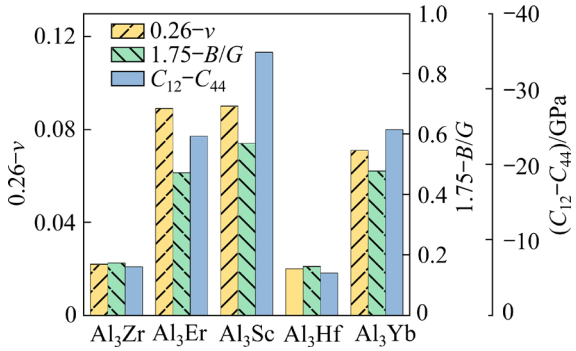

Fig. 2 Brittleness and ductility analysis of $L1_2$-Al_3X structural phases

$$H_V=\frac{(1-2\nu)E}{6(1+\nu)} \tag{11}$$

There exists a disparity between the calculated hardness and the real hardness. However, it is possible to horizontally compare the relationship between the hardness of each structural phase. Based on the findings depicted in Fig. 3, the hardness of the structural phase is arranged from large to small as follows: Al_3Sc, Al_3Er, Al_3Yb, Al_3Zr and Al_3Hf. Based on the findings reported in the literature [15,66], the hardness of structural phases follows the order of Al_3Sc, Al_3Er and Al_3Yb, which is consistent with the calculation results. The analysis reveals an association between hardness and brittleness tendency. A high hardness in the structural phase corresponds to the strong brittleness tendency. A low hardness corresponds to the weak brittleness tendency.

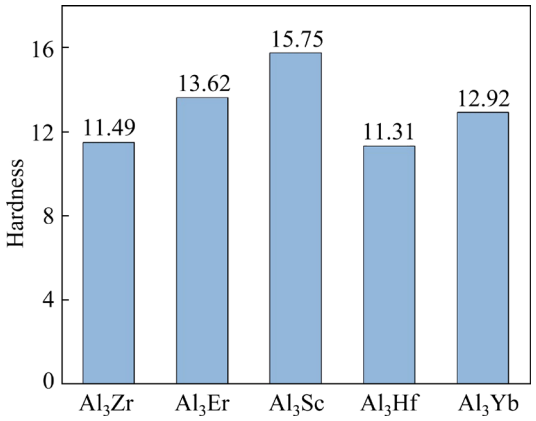

Fig. 3 Hardness of $L1_2$-Al_3X structural phases

3.5 Thermodynamic properties

The thermodynamic stability of $L1_2$-Al_3X structural phases was assessed using various thermodynamic properties, including Helmholtz free energy, specific heat, entropy and enthalpy, as shown in Eqs. (12)−(17) [67]:

$$F(V,T)=E_0(V)+F_{\mathrm{el}}(V,T)+F_{\mathrm{vib}}(V,T) \tag{12}$$

$$F_{\mathrm{vib}}(V,T)=\int_0^{\infty}\left[\hbar\omega/2+k_{\mathrm{B}}T\ln\left(1-\mathrm{e}^{-\hbar\omega/k_BT}\right)\right]\cdot g(\omega,V)\,\mathrm{d}\omega \tag{13}$$

$$c_p(p,T)=-T\frac{\partial^2\min\limits_V\left[F(V,T)+pV\right]}{\partial T^2} \tag{14}$$

$$c_v=\left(\partial U/\partial T\right)_V \tag{15}$$

$$S=-\partial F/\partial T \tag{16}$$

$$H=F+TS \tag{17}$$

where $F(V, T)$ is the Helmholtz free energy, $E_0(V)$ is the ground state primitive cell energy at 0 K, $F_{\mathrm{el}}(V, T)$ is the thermal electronic contribution, $F_{\mathrm{vib}}(V, T)$ is the vibrational contribution of lattice, $\hbar$ is the reduced Planck constant, ω is the phonon vibration frequency, k_{B} is the Boltzmann constant, c_p is the specific heat capacity at constant pressure, c_v is the specific heat capacity at constant volume, S is the entropy, H is the enthalpy, p is pressure, V is the volume, U is the internal energy, and T is the temperature.

The temperature range of 200−600 K was selected for the service environment of heat-resistant Al conductors. In this particular range, the influence of free electrons on specific heat was neglected. Figure 4 displays the computed thermodynamic parameters for the $L1_2$-Al_3X structural phases. As shown in Fig. 4(a), the experimentally determined specific heat capacity at constant pressure of Al_3Sc shows a high level of concordance with the calculated values [68]. Figure 4(b) illustrates the specific heat capacity at constant volume. As the temperature rises, there is a steady deceleration in the increasing rate of specific heat until it reaches the Dulong−Petit limit. This observation aligns with the principle governing the alteration of specific heat capacity at constant volume conditions in crystalline solids [69]. All of the above verify the accuracy and reliability of the calculation results in this paper.

As shown in Fig. 4(c), it can be observed that the Helmholtz free energy exhibits a decreasing trend as the temperature increases. This finding provides evidence for the high stability and spontaneous formation of these structural phases.

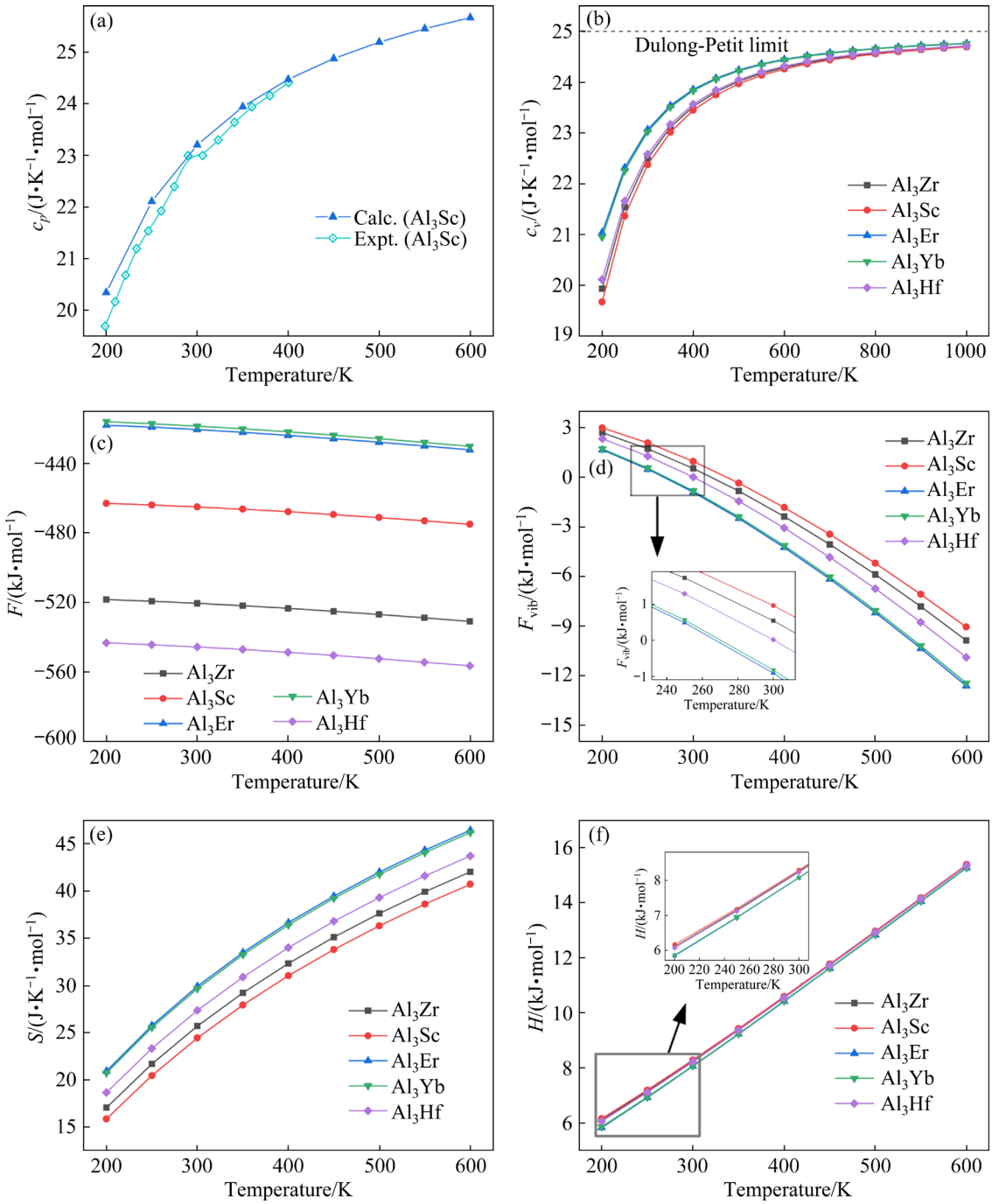

Fig. 4 Thermodynamic properties for L1$_2$-Al$_3$X structural phases (Insets show the locally enlarged plots): (a) c_p comparison between calculated and experimental data; (b) Specific heat capacity at constant volume (c_v); (c) Helmholtz free energy (F); (d) Helmholtz vibration free energy (F_{vib}); (e) Entropy (S); (f) Enthalpy (H)

The thermodynamic stability of structural phases was further analyzed by studying the effect of temperature on the Helmholtz vibrational free energy (Fig. 4(d)). At lower temperatures (200−400 K), the Helmholtz vibrational free energy exhibits a somewhat slower rate of decrease. At higher temperatures (400−600 K), the decrease rate of the free energy gradually increases. In the temperature range of f 200−600 K, the Helmholtz vibrational free energy of phase from large to small is Al$_3$Sc, Al$_3$Zr, Al$_3$Hf, Al$_3$Yb and Al$_3$Er, with similar values for Al$_3$Yb and Al$_3$Er. The system tends to approach a state of thermodynamic equilibrium (maximum entropy), as indicated by the variation curve of the entropy with temperature (Fig. 4(e)). This is due to the increased intensity of

lattice vibrations. The entropy exhibits a progressive increase as the temperature increases, and this rate of increase gradually diminishes. The entropy values of the structural phases, in descending order, are Al_3Er, Al_3Yb, Al_3Hf, Al_3Zr and Al_3Sc. Finally, the enthalpy of $L1_2$-Al_3X structural phases was investigated (Fig. 4(f)). It was observed that the variations in enthalpy between the different structural phases are minimal in response to temperature change. The enthalpy progressively rises with temperature, improving the thermodynamic stability of structural phase.

It is commonly recognized that throughout the heating process, the structural phases exhibit great thermodynamic stability when there is a low Helmholtz vibrational free energy, higher entropy, and higher enthalpy increasing. The structural phases exhibiting notable thermodynamic stability were identified as Al_3Er and Al_3Yb, afterwards succeeded by Al_3Hf, Al_3Zr and Al_3Sc. Additionally, the degree of lattice vibration of the heated crystal can be precisely represented by the thermal expansion coefficient. The low coefficient value represents a small degree of vibration, which suggests strong thermodynamic stability. The thermal expansion coefficients of the structural phases at 300 K, from big to small, are Al_3Sc, Al_3Zr, Al_3Hf, Al_3Yb and Al_3Er, based on findings published in the literature [15,17,70]. This confirms the thermodynamic stability calculation results even further.

3.6 Electronic structures

To evaluate the chemical bond properties of the $L1_2$-Al_3X phases, the electronic state around the Fermi level was measured after the Fermi level of the energy band structure situated at 0 (Fig. 5).

The conduction bands of the various structural phases exhibit several intersections with the Fermi level and pass through it multiple times. Every phase exhibits some conductivity and obvious properties of metallic bonds because they are not zero at the Fermi level. The Al_3Zr (Fig. 5(a)) and Al_3Hf (Fig. 5(d)) phases exhibit a greater number of crossings with the Fermi level in compared to the other phases. The energy band variation reveals that the energy bands of Al_3Er (Fig. 5(b)), Al_3Sc (Fig. 5(c)) and Al_3Yb (Fig. 5(e)) display distinct parabolic profiles at the conduction and valence band in proximity to the Fermi level. This suggests that the properties of covalent bonds are present.

Figure 6 displays the density of states (DOS) for $L1_2$-Al_3X structural phases. The DOS of Al_3Zr (Fig. 6(a)) mostly arises from the hybridization of Al 3s, Al 3p and Zr 4d electrons close to the Fermi level. The energy range between −10 and −4 eV predominantly consists of an Al−Al bond, which is primarily provided by Al 3s orbital. The energy range between −4 and 0 eV is characterized by a hybrid bond of Al 3p and Zr 4d. In addition to the Zr−Zr bond, a robust Al−Zr hybrid bond is observed in the higher energy region located above the Fermi level. The orbitals of valence electrons in adjacent atoms undergo overlapping, resulting in the formation of bonding and anti-bonding states. When an overlap occurs, a visible pseudogap is formed, and the system's covalent bond strength is determined by the gap's breadth. The Fermi surface is situated adjacent to the anti-bonding states within the lower region of the pseudogap valley. Since the corresponding DOS exhibits a high value, there is an increased population of electrons crossing the Fermi level.

The bond properties of other $L1_2$-Al_3X structural phases (Figs. 6(b)−(e)) in the Fermi level are similar to Al_3Zr. Among the aforementioned compounds, it is worth noting that the Fermi surface of Al_3Hf is also positioned adjacent to the antibonding peak. Al_3Er, Al_3Sc, and Al_3Yb show strong local stability because their Fermi surfaces are located toward the bottom of the pseudogap valley and their DOS is comparatively tiny. Simultaneously, the observed pseudogap has a significant width, suggesting the presence of robust hybrid bonds among Al−Er, Al−Sc and Al−Yb. They are the obvious properties of covalent bonds and the reason why the hardness and brittleness of Al_3Er, Al_3Yb and Al_3Sc are higher than those of Al_3Zr and Al_3Hf.

The metallicity (f_m) of the structural phase was determined by Eq. (18) [71]:

$$f_m = \frac{0.026 D_f}{n_e} \tag{18}$$

where D_f is the DOS at the Fermi level, and n_e is the valence electron density in the unit cell. The f_m values of Al_3Hf, Al_3Er, Al_3Zr, Al_3Yb and Al_3Sc are 0.1662, 0.1507, 0.1609, 0.1543 and 0.1254, respectively. The metallicity of Al_3Hf and Al_3Zr are more prominent, which is consistent with the previous

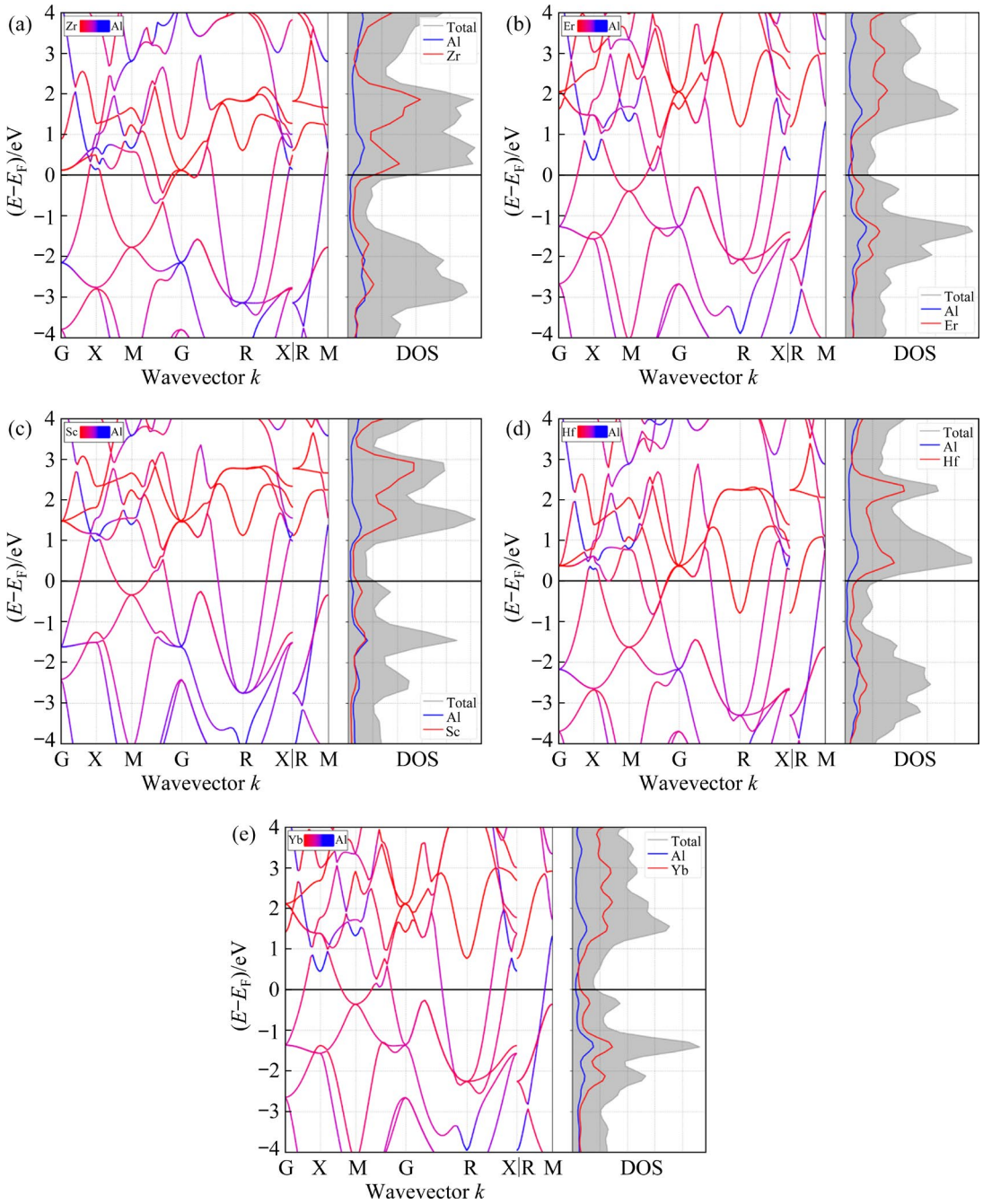

Fig. 5 Band structures of $L1_2$-Al_3X structural phases: (a) Al_3Zr; (b) Al_3Er; (c) Al_3Sc; (d) Al_3Hf; (e) Al_3Yb

analysis of the properties of metal bonds. It can be proved that the electrical conductivities of Al_3Hf and Al_3Zr are stronger than those of Al_3Er, Al_3Yb and Al_3Sc.

3.7 Charge density and differential charge density

It is evident that the charge distribution surrounding each atom in each phase is spherical from the charge density of the $L1_2$-Al_3X phase on the (001) plane (Fig. 7). The X atom is surrounded by a significant quantity of electrons, suggesting that all the structural phases display the typical properties of metallic bonds.

By examining the form and distribution of the difference charge density in the structural phases on the (001) plane, it is possible to determine that the atoms exhibit mixed properties of bonds following redistribution (Fig. 8).

It is the aluminum atom that loses electrons in each structural phase. (blue region in Fig. 8). Additionally, certain electrons tend to congregate around X atoms (red and yellow regions in Fig. 8). This accumulation of electrons leads to the formation

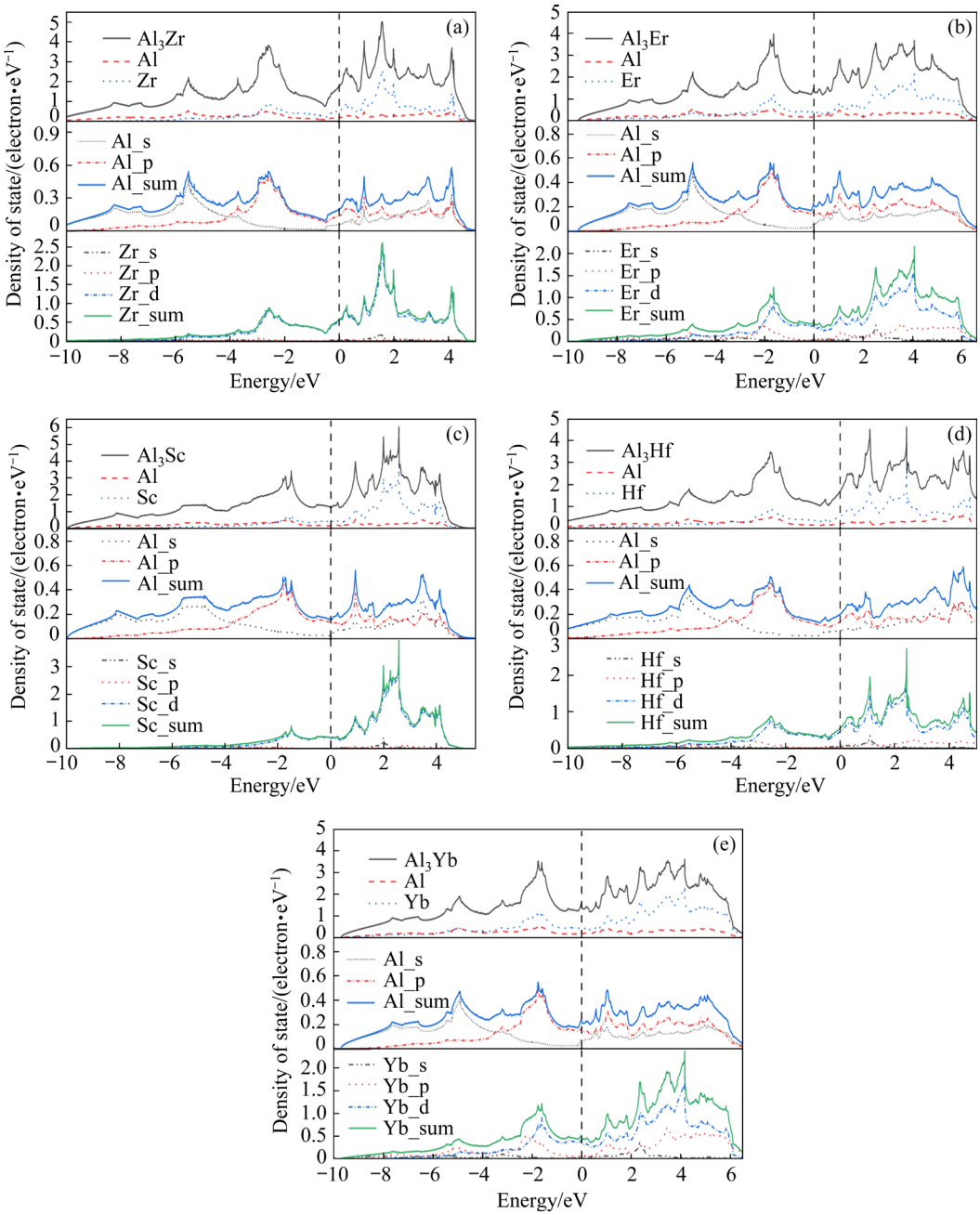

Fig. 6 Total density of states (TDOS) and partial density of states (PDOS) of $L1_2$-Al_3X structural phases (Vertical dashed line is Fermi level E_F (0 eV)): (a) Al_3Zr; (b) Al_3Er; (c) Al_3Sc; (d) Al_3Hf; (e) Al_3Yb

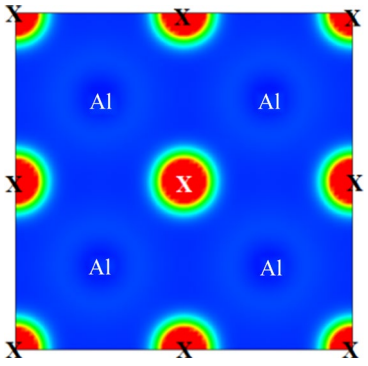

Fig. 7 Charge density of $L1_2$-Al_3X structural phases

of ionic bonds, exemplified by compounds such as Al_3Zr, Al_3Sc and Al_3Hf. Furthermore, it has been seen that certain electrons participate in the formation of robust, directed covalent bonds between Al and X atoms. The analysis demonstrates that the orbital hybridization between Al and X atoms results in the formation of overlapping electron clouds between Al and X. However, there is not much charge distortion at the junction of the two atoms, indicating that the metallic bonds of the structural phases remain maximally dominating.

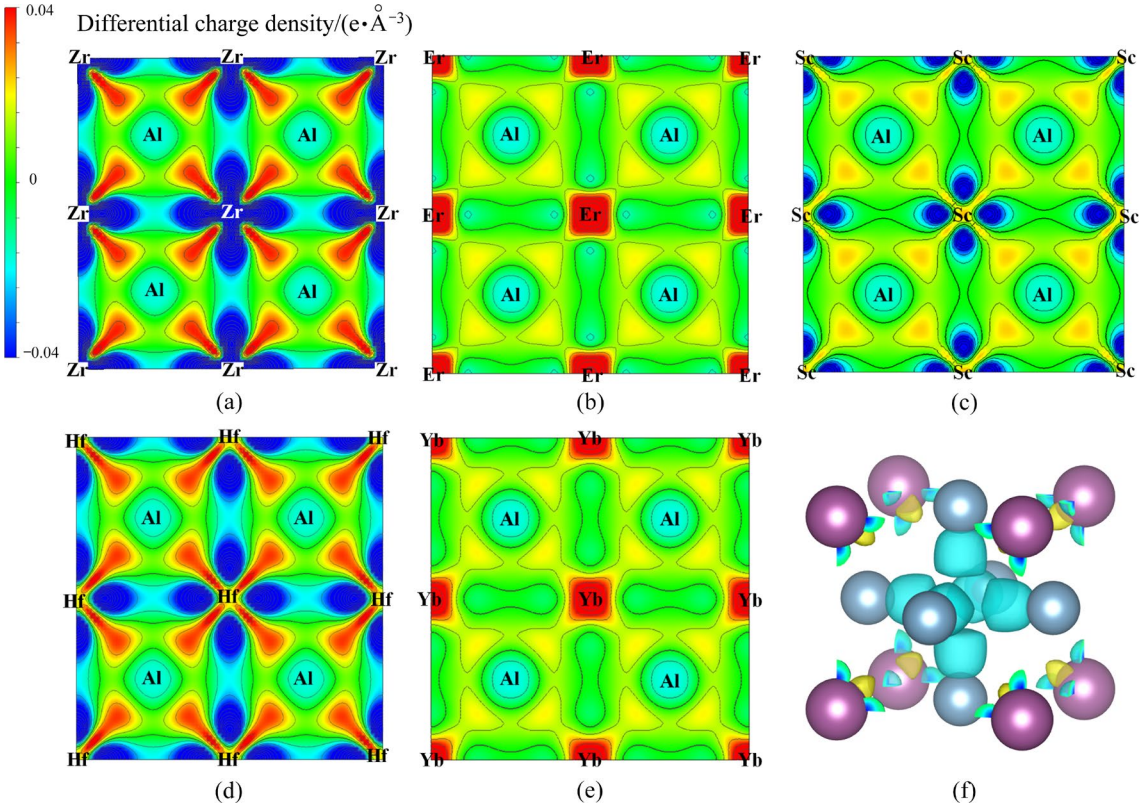

Fig. 8 Difference charge density of $L1_2$-Al_3X structural phases: (a) Al_3Zr; (b) Al_3Er; (c) Al_3Sc; (d) Al_3Hf; (e) Al_3Yb; (f) 3D distribution of $L1_2$-Al_3X

Upon further examination, it has been determined that the compounds Al_3Sc, Al_3Er and Al_3Yb exhibit the presence of covalent bonds among Al−Sc, Al−Er and Al−Yb. The thermodynamic stability of the structural phases increases with the increase of covalent bond strength, leading to enhanced the strength and brittleness of phases. It is important to highlight that Al_3Sc has the characteristics of covalent bonds but lacks thermodynamic stability. This is due to the existence of a certain amount of ionic bonds in Al_3Sc. Compared with covalent bonds, ionic bonds are susceptible to the influence of thermal shock, leading to inadequate thermal shock resistance. This has an adverse effect on the thermodynamic stability of Al_3Sc [72]. It is discovered that the thermodynamic stability of $L1_2$-Al_3X phases in aluminum alloy increases with the increase of X atom radius [16]. The structural phases of Al_3Hf and Al_3Zr exhibit comparable covalent bond characteristics. To some extent, though, Al_3Hf exhibits more thermodynamic stability than Al_3Zr because of the comparatively larger atomic radius of the Hf atoms.

4 Conclusions

(1) The alloy forming ability of the phases from strong to weak is Al_3Zr, Al_3Sc, Al_3Er, Al_3Yb and Al_3Hf, and the structural stability of the phases from strong to weak is Al_3Zr, Al_3Hf, Al_3Er, Al_3Sc and Al_3Yb.

(2) All structural phases meet the requirements of cubic phase mechanical stability. Al_3Zr, Al_3Hf and Al_3Sc have higher shear and deformation resistance than Al_3Er and Al_3Yb, where Al_3Er, Al_3Sc and Al_3Yb exhibit higher brittleness than Al_3Zr and Al_3Hf. The phase hardness from large to small is Al_3Sc, Al_3Er, Al_3Yb, Al_3Zr and Al_3Hf.

(3) In the temperature range of 200−600 K, Al_3Er and Al_3Yb have the highest thermal stability, followed by Al_3Hf, Al_3Zr and Al_3Sc.

(4) All structural phases exhibit the substantial metallic properties, indicating their good electrical conductivities. Al_3Hf and Al_3Zr have greater electrical conductivities than Al_3Er, Al_3Yb, and Al_3Sc.

(5) The covalent bond characteristics in Al_3Sc,

Al_3Er and Al_3Yb help to improve the hardness, brittleness and thermodynamic stability of the structural phases. The thermodynamic stability of Al_3Sc is significantly reduced bonds.

CRediT authorship contribution statement

Yao-jie KONG: Conceptualization, Methodology, Investigation, Formal analysis, Writing − Original draft; **Hong-ying LI:** Conceptualization, Supervision, Funding acquisition, Writing – Reviewing and editing; **Hui-jin TAO:** Supervision, Writing – Reviewing and editing; **Wen-jian LIU:** Writing – Reviewing and editing.

Declaration of competing interest

The authors declare that they have no known competing financial interests or personal relationships that could have appeared to influence the work reported in this paper.

Acknowledgments

This work was supported by the National Natural Science Foundation of China (No. 52274403).

References

[1] LIU Li, JIANG Jian-tang, CUI Xiang-yuan, ZHANG Bo, ZHEN Liang, RINGER S P. Correlation between precipitates evolution and mechanical properties of Al−Sc−Zr alloy with Er additions [J]. Journal of Materials Science & Technology, 2022, 99: 61−72.

[2] WANG Yu, ZHU Lang-jie, NIU Guo-dong, MAO Jian. Conductive Al alloys: The contradiction between strength and electrical conductivity [J]. Advanced Engineering Materials, 2021, 23(5): 2001249.

[3] ZHANG Jia-yi, PENG Jing. A review on aluminum alloy conductors influenced by alloying elements and thermo-mechanical treatments: Microstructure and properties [J]. Journal of Materials Research, 2023, 38(6): 1488−1509.

[4] LI Hong-ying, GAO Zhao-he, YIN Hao, JIANG Hao-fan, SU Xiong-jie, BIN Jie. Effects of Er and Zr additions on precipitation and recrystallization of pure aluminum [J]. Scripta Materialia, 2013, 68(1): 59−62.

[5] KNIPLING K E, DUNAND D C, SEIDMAN D N. Criteria for developing castable, creep-resistant aluminum-based alloys—A review [J]. International Journal of Materials Research, 2022, 97(3): 246−265.

[6] JIANG Sheng-yu, WANG Rui-hong. Manipulating nanostructure to simultaneously improve the electrical conductivity and strength in microalloyed Al−Zr conductors [J]. Scientific Reports, 2018, 8(1): 6202.

[7] GAO Zhao-he, LI Hong-ying, LAI Yong-qiu, OUYANG Xun, LI De-wang. Effects of minor Zr and Er on microstructure and mechanical properties of pure aluminum [J]. Materials Science and Engineering A, 2013, 580: 92−98.

[8] DESCHAMPS A, LAE L, GUYOT P. In situ small-angle scattering study of the precipitation kinetics in an Al−Zr−Sc alloy [J]. Acta Materialia, 2007, 55(8): 2775−2783.

[9] HALLEM H, FORBORD B, MARTHINSEN K. An investigation of dilute Al−Hf and Al−Hf−Si alloys [J]. Materials Science and Engineering A, 2004, 387: 940−943.

[10] LI Hong-ying, LI De-wang, ZHU Zhi-xiang, CHEN Bao-an, CHEN Xin, YANG Chang-long, ZHANG Hong-yu, KANG Wei. Grain refinement mechanism of as-cast aluminum by hafnium [J]. Transactions of Nonferrous Metals Society of China, 2016, 26(12): 3059−3069.

[11] ZHANG Yong-zhi, ZHOU Wei, GAO Hai-yan, HAN Yan-feng, WANG Kai, WANG Jun, SUN Bao-de, GU Sun-wang, YOU Wei-ren. Precipitation evolution of Al−Zr−Yb alloys during isochronal aging [J]. Scripta Materialia, 2013, 69(6): 477−480.

[12] SAHA S, TODOROVA T Z, ZWANZIGER J W. Temperature dependent lattice misfit and coherency of Al_3X (X= Sc, Zr, Ti and Nb) particles in an Al matrix [J]. Acta Materialia, 2015, 89: 109−115.

[13] WANG Hai-sheng, MIN Jie, WANG Hong-jun. Microstructure and electrical conductivity of Al alloy wire with Zr and Ce [J]. Chinese Journal of Rare Metals, 2020, 44(7): 716−721. (in Chinese)

[14] GHOSH G, ASTA M. First-principles calculation of structural energetics of Al−TM (TM=Ti, Zr, Hf) intermetallics [J]. Acta Materialia, 2005, 53(11): 3225−3252.

[15] PAN Rong-kai, WANG Hai-chen, SHI Tao-tao, TIAN Xiao, TANG Bi-yu. Thermal properties and thermoelasticity of $L1_2$ ordered Al_3RE (RE=Er, Tm, Yb, Lu) phases: A first-principles study [J]. Materials & Design, 2016, 102: 100−105.

[16] LAN Ji-hang, CHEN Zhao-qun, LIU Ling-hong, ZHANG Qing-zhou, HE Meng-dong, LI Jian-bo, PENG Xiao-peng, FAN Tou-wen. The thermal properties of $L1_2$ phases in aluminum enhanced by alloying elements [J]. Metals, 2021, 11(9): 1420.

[17] FAN Tou-wen, RUAN Zi-xiong, HU Te, WANG Kai, DUAN Shi-yun, DENG Yuan-xiang, TANG Ping-ying, WU Yuan-zhi. High-throughput first-principles study of physical properties of $L1_2$-Al_3M particles [J]. Materials Today Communications, 2022, 31: 103748.

[18] CUI Yang, LI Shou-hang, YING Tao, BAO Hua, ZENG Xiao-qin. Research on the thermal conductivity of metals based on first principles [J]. Acta Metallurgica Sinica, 2021, 57(3): 375−384. (in Chinese)

[19] WANG Yu, WANG Jun-sheng, XUE Cheng-peng, WANG Shuo, CHEN Dong-xu, ZHANG Chi. Review of microalloying effects on high temperature Al_3X precipitates in Al alloys [J]. Aeronautical Manufacturing Technology, 2021, 64(15): 68−77, 85. (in Chinese)

[20] KRESSE G, FURTHMÜLLER J. Efficiency of ab-initio total energy calculations for metals and semiconductors using a plane-wave basis set [J]. Computational Materials Science, 1996, 6(1): 15−50.

[21] KRESSE G, FURTHMÜLLER J. Efficient iterative schemes for ab initio total-energy calculations using a plane-wave basis set [J]. Physical Review B, 1996, 54(16): 11169−11186.

[22] PERDEW J P, BURKE K, ERNZERHOF M. Generalized gradient approximation made simple [J]. Physical Review Letters, 1996, 77(18): 3865−3868.

[23] BLÖCHL P E. Projector augmented-wave method [J]. Physical Review B, 1994, 50(24): 17953−17979.

[24] SVANE A, TEMMERMAN W M, SZOTEK Z, PETIT L, STRANGE P, WINTER H. Ab initio theory of valency in ytterbium compounds [J]. Physical Review B, 2000, 62(20): 13394−13399.

[25] HUANG Fu-hao, WANG Zi-long, LIU Yong-li, MENG Fan-shun, SONG Jiu-peng, QI Yang. A first principles investigation of W1-X IrX alloys: Structural, electronic, mechanical, and thermal properties [J]. Acta Metallurgica Sinica, 2022, 58(2): 231−240. (in Chinese)

[26] YU Wei, CHONG Xiao-yu, GAN Meng-di, WEI Yan, ZHANG Ai-min, HU Chang-yi, FENG Jing. Effect of alloying elements on thermoelastic properties of Pt-based alloys [J]. Transactions of Nonferrous Metals Society of China, 2023, 33(6): 1851−1861.

[27] LI Run-yue, DUAN Yong-hua. Electronic structures and thermodynamic properties of $HfAl_3$ in $L1_2$, $D0_{22}$ and $D0_{23}$ structures [J]. Transactions of Nonferrous Metals Society of China, 2016, 26(9): 2404−2412.

[28] GHOSH G, VAYNMAN S, ASTA M, FINE M E. Stability and elastic properties of $L1_2$-$(Al,Cu)_3(Ti,Zr)$ phases: Ab initio calculations and experiments [J]. Intermetallics, 2007, 15(1): 44−54.

[29] REN Zhi-xin, QIN Jia-qian, LIU Ri-ping, ZHANG Xin-yu. Vacancy mediated alloying strengthening effects on Al/Al_3Zr interface and stabilization of $L1_2$-Al_3Zr: A first-principles study [J]. Journal of Alloys and Compounds, 2020, 825: 153825.

[30] ZHANG Chao-ming, JIANG Yong, CAO Fu-hua, HU Tao, WANG Yi-ren, YIN Deng-feng. Formation of coherent, core-shelled nano-particles in dilute Al−Sc−Zr alloys from the first-principles [J]. Journal of Materials Science & Technology, 2019, 35(5): 930−938.

[31] DESCH P B, SCHWARZ R B, NASH P. Formation of metastable $L1_2$ phases in Al_3Zr and Al−12.5%X−25%Zr (X≡Li, Cr, Fe, Ni, Cu) [J]. Journal of the Less Common Metals, 1991, 168(1): 69−80.

[32] YANG Tian-xing, WEI Ming-zhi, DING Zong-ye, HAN Xiu-jun, LI Jiang-guo. First-principle calculations on the $Al/L1_2$-Al_3Zr heterogeneous nucleation interface [J]. Calphad, 2020, 69: 101768.

[33] ZHANG Chao-min, XIE Pan, JIANG Yong, ZHAN Shen, MING Wen-quan, CHEN Jiang-hua, SONG Ke-xing, ZHANG Hao. Double-shelled $L1_2$ nano-structures in quaternary Al−Er−Sc−Zr alloys: Origin and critical significance [J]. Acta Metallurgica Sinica (English Letters), 2021, 34(9): 1277−1284.

[34] SUN Shun-ping, LI Xiao-ping, YANG Jie, WANG Hong-jin, JIANG Yong, YI Dan-qing. Point defect concentrations of $L1_2$-Al_3X(Sc,Zr,Er) [J]. Rare Metals, 2018, 37(8): 699−706.

[35] GAO Chun-lai, GAO Kun-yuan, DING Yu-sheng, LI Hao-nan, WU Xiao-lan, WEN Sheng-ping, GAO Mu, HUANG Hui, NIE Zuo-ren, ZHOU De-jing. The phase stability of Al_3Er studied by the first-principles calculations and experimental analysis [J]. Metals, 2021, 11(5): 759.

[36] van VUCHT J H N, BUSCHOW K H J. The structures of the rare-earth trialuminides [J]. Journal of the Less Common Metals, 1966, 10(2): 98−107.

[37] CANNON J F, HALL H T. Effect of high pressure on the crystal structures of lanthanide trialuminides [J]. Journal of the Less Common Metals, 1975, 40(3): 313−328.

[38] WOODWARD C, ASTA M, KRESSE G, HAFNER J. Density of constitutional and thermal point defects in $L1_2$ Al_3Sc [J]. Physical Review B, 2001, 63(9): 094103.

[39] MAO Zu-gang, CHEN Wei, SEIDMAN D N, WOLVERTON C. First-principles study of the nucleation and stability of ordered precipitates in ternary Al−Sc−Li alloys [J]. Acta Materialia, 2011, 59(8): 3012−3023.

[40] WANG Yu, MENG Ya-nan, WANG Jun-sheng, ZHANG Chi, HUANG Hou-bing. Mechanical properties of defective $L1_2$-Al_3X (X=Sc, Lu) phase: A first-principles study [J]. Journal of Rare Earths, 2021, 39(2): 217−224.

[41] COLINET C, PASTUREL A. Phase stability and electronic structure in $ZrAl_3$ compound [J]. Journal of Alloys and Compounds, 2001, 319(1/2): 154−161.

[42] HU Zhi, YIN Zheng, LIN Jing-wu, ZHANG Ling-yan, QIU Shui-chai, YAN Hong, LUO Chao, SONG Hong-gun. Microstructural, electronic, and mechanical properties of $L1_2$ ordered Al_3Er and Al_3Yb intermetallics: An experimental and first-principles calculations [J]. Materials Research Express, 2019, 6(11): 116516.

[43] KOMSA H P, KRASHENINNIKOV A V. Native defects in bulk and monolayer MoS_2 from first principles [J]. Physical Review B, 2015, 91(12): 125304.

[44] ZUBOV V I, TRETIAKOV N P, RABELO J N T, ORTIZ J F S. Calculations of the thermal expansion, cohesive energy and thermodynamic stability of a Van der Waals crystal-fullerene C_{60} [J]. Physics Letters A, 1994, 194(3): 223−227.

[45] WANG Na, TANG Bi-yu. Structural, elastic and electronic properties of $L1_2$ aluminum phases from first principles calculation [J]. Acta Physica Sinica, 2009, 58(13): 230−234. (in Chinese)

[46] ZHANG Xu-dong, WANG Shao-qing. First-principles investigation of the thermodynamics properties of Al_3Sc and Al_3Zr intermetallics [J]. Acta Metallurgica Sinica, 2013, 49(4): 501−505. (in Chinese)

[47] MEDVEDEVA N I, GORNOSTYREV Y N, NOVIKOV D L, MRYASOV O N, FREEMAN A J. Ternary site preference energies, size misfits and solid solution hardening in NiAl and FeAl [J]. Acta Materialia, 1998, 46(10): 3433−3442.

[48] VINET P, ROSE J H, FERRANTE J, SMITH J R. Universal features of the equation of state of solids [J]. Journal of Physics: Condensed Matter, 1989, 1(11): 1941−1963.

[49] ZHANG Xu-dong, JIANG Wei. First-principles investigations on vibrational, thermodynamic, mechanical properties and thermal conductivity of $L1_2$ Al_3X (X = Sc, Er, Tm, Yb) intermetallics [J]. Physica Scripta, 2015, 90(6): 065701.

[50] TAO Xiao-ma, OUYANG Yi-fang, LIU Hua-shan, FENG Yuan-ping, DU Yong, JIN Zhan-peng. First-principles calculations of the thermodynamic and elastic properties of the $L1_2$-based Al_3RE (RE = Sc, Y, La−Lu) [J]. International Journal of Materials Research, 2008, 99: 582−588.

[51] DUAN Yong-hua, WU Zhao-yong, HUANG Bo, CHEN Shuai. Phase stability and anisotropic elastic properties of the Hf−Al intermetallics: A DFT calculation [J]. Computational Materials Science, 2015, 110: 10−19.

[52] GAO M C, ROLLETT A D, WIDOM M. Lattice stability of aluminum−rare earth binary systems: A first-principles approach [J]. Physical Review B, 2007, 75(17): 174120.

[53] FU Chong-long, WANG Xin-dong, YE Yi-ying, HO K M. Phase stability, bonding mechanism, and elastic constants of Mo_5Si_3 by first-principles calculation [J]. Intermetallics, 1999, 7(2): 179−184.

[54] JAMAL M, ASADABADI S J, AHAMD I, ALIABAD H A R. Elastic constants of cubic crystals [J]. Computational Materials Science, 2014, 95: 592−599.

[55] YANG Qiang, LIU Xiao-juan, BU Fan-qiang, MENG Fan-zhi, ZHENG Tian, ZHANG De-ping, MENG Jian. First-principles phase stability and elastic properties of Al−La binary system intermetallic compounds [J]. Intermetallics, 2015, 60: 92−97.

[56] TIAN Tian, WANG Xiu-feng, LI Wen. Ab initio calculations on elastic properties in $L1_2$ structure Al_3X and X_3Al-type (X=transition or main group metal) intermetallic compounds [J]. Solid State Communications, 2013, 156: 69−75.

[57] HYLAND R W, STIFFLER R C. Determination of the elastic constants of polycrystalline Al_3Sc [J]. Scripta Metallurgica et Materialia, 1991, 25(2): 473−477.

[58] BORN M, HUANG Kun. Dynamical theories of crystal lattices [M]. New York: Oxford University Press, 1956.

[59] BOND W L. Physical properties of crystals: Their representation by tensors and matrices [J]. Journal of Physics and Chemistry of Solids, 1957, 3(3/4): 338.

[60] HU Hai, ZHAO Ming-qi, WU Xiao-zhi, JIA Zhi-hong, WANG Rui, LI Wei-guo, LIU Qing. The structural stability, mechanical properties and stacking fault energy of Al_3Zr precipitates in Al−Cu−Zr alloys: HRTEM observations and first-principles calculations [J]. Journal of Alloys and Compounds, 2016, 681: 96−108.

[61] BAKARE F, BABALOLA M I, IYORZOR B E. The role of alloying elements on the structural, mechanical and thermodynamic properties of Al_3X binary alloy system (X= Mg, Sc and Zr): First principle calculations [J]. Materials Research Express, 2017, 4(11): 116502.

[62] DUAN Yong-hua, SUN Yong, PENG Ming-jun, ZHOU Sheng-gang. Ab-initio investigations on elastic properties in $L1_2$ structure Al_3Sc and Al_3Y under high pressure [J]. Journal of Alloys and Compounds, 2014, 585: 587−593.

[63] FU Chong-long. Electronic, elastic, and fracture properties of trialuminide alloys: Al_3Sc and Al_3Ti [J]. Journal of Materials Research, 1990, 5(5): 971−979.

[64] WU Ying, MA Li-shi, ZHOU Xiao-long, DUAN Yong-hua, SHEN Li, PENG Ming-jun. Insights to electronic structures, elastic properties, fracture toughness, and thermal properties of $M_{23}C_6$ carbides [J]. International Journal of Refractory Metals and Hard Materials, 2022, 109: 105985.

[65] PUGH S F. Relations between the elastic moduli and the plastic properties of polycrystalline pure metals [J]. The London, Edinburgh, and Dublin Philosophical Magazine and Journal of Science, 1954, 45(367): 823−843.

[66] LIU Xiao-min, WANG Qang, ZHAO Chuan, LI Hong-ping, WANG Ming-liang, CHEN Dong, WANG Hao-wei. Formation of ordered precipitates in Al−Sc−Er−(Si/Zr) alloy from first-principles study [J]. Journal of Rare Earths, 2021, 39(5): 609−620.

[67] TOGO A, TANAKA I. First principles phonon calculations in materials science [J]. Scripta Materialia, 2015, 108: 1−5.

[68] GUPTA A, KAVAKBASI B T, DUTTA B, GRABOWSKI B, PETERLECHNER M, HICKEL T, DIVINSKI S V, WILDE G, NEUGEBAUER J. Low-temperature features in the heat capacity of unary metals and intermetallics for the example of bulk aluminum and Al_3Sc [J]. Physical Review B, 2017, 95(9): 094307.

[69] DEMIROGLU I, SEVIK C. Extraordinary negative thermal expansion of two-dimensional nitrides: A comparative ab initio study of quasiharmonic approximation and molecular dynamics simulations [J]. Physical Review B, 2021, 103(8): 085430.

[70] FEREIDONNEJAD R, OSTOVARI M A, MOADDELI M. Modified embedded-atom method interatomic potentials for Al−Ti, Al−Ta, Al−Zr, Al−Nb and Al−Hf binary intermetallic systems [J]. Computational Materials Science, 2022, 213: 111685.

[71] WANG Peng, LI Jun, LIN Chong-zhi, YANG Liu, PENG Lin, WANG Ying, XIAO Cong, CHEN Jing-chao. First-principles calculations of electronic structure and mechanical properties of Ti−Ni intermetallic compounds [J]. The Chinese Journal of Nonferrous Metals, 2016, 26(12): 2546−2554. (in Chinese)

[72] GAO Fa-ming, ZHANG Si-yuan. Relationship of chemical bond and thermal expansion in crystals [J]. Journal of Synthetic Crystals, 1992, 21(4): 325−328. (in Chinese)

耐热铝导体的 $L1_2$-Al_3X 结构相物理性质的第一性原理研究

孔耀颉[1]，李红英[1,2,3]，陶辉锦[1]，刘文鉴[1]

1. 中南大学 材料科学与工程学院，长沙 410083；
2. 中南大学 轻质高强结构材料国家重点实验室，长沙 410083；
3. 中南大学 有色金属材料科学与工程教育部重点实验室，长沙 410083

摘　要：采用第一性原理研究铝导体中 $L1_2$-Al_3X (X=Zr, Sc, Er, Yb, Hf)结构相的力学、热力学和导电性能。结果表明，所有结构相都有良好的合金化能力和结构稳定性，其中 Al_3Zr 表现最好；Al_3Zr、Al_3Hf 和 Al_3Sc 具有更强的抗剪切和变形能力；在 200~600 K 内，Al_3Er 和 Al_3Yb 的热稳定性最好，其次是 Al_3Hf、Al_3Zr 和 Al_3Sc；结构相均表现出较强的金属性，证明具有一定的导电能力，Al_3Hf 和 Al_3Zr 的导电能力强于 Al_3Er、Al_3Yb 和 Al_3Sc；Al_3Sc、Al_3Er 和 Al_3Yb 中的共价键特性有利于提高结构相的硬度、脆性和热稳定性，Al_3Sc 由于离子键的存在大幅降低了自身的热稳定性。

关键词：铝导体；$L1_2$-Al_3X 结构相；第一性原理；力学性能；热力学性质；导电性；价键

(Edited by Xiang-qun LI)